Eur. Phys. J. Spec. Top.
https://doi.org/10.1140/epjs/s11734-025-01920-5

THE EUROPEAN PHYSICAL JOURNAL SPECIAL TOPICS

Regular Article

Measuring adhesion of soft elastic shells

Miguel Trejo[1,a], Suomi Ponce[2,b], José Bico[2,c], Étienne Reyssat[2,d], Benoît Roman[2,e], and Chung-Yuen Hui[3,f]

[1] Instituto de Física de Buenos Aires (IFIBA-CONICET), Departamento de Física, Facultad de Ciencias Exactas y Naturales, Universidad de Buenos Aires, Ciudad Universitaria, C1428 Buenos Aires, Argentina
[2] Laboratoire de Physique et Mécanique des Milieux Hétérogènes PMMH, CNRS, ESPCI Paris, Université PSL, Sorbonne Université, Université Paris Cité, 75005 Paris, France
[3] Department of Mechanical and Aerospace Engineering, Field of Theoretical and Applied Mechanics, Cornell University, Ithaca, NY 14853, USA

Received 2 September 2025 / Accepted 4 September 2025
© The Author(s), under exclusive licence to EDP Sciences, Springer-Verlag GmbH Germany, part of Springer Nature 2025

Abstract Adhesion of soft materials is commonly measured through the classical JKR framework where a full elastic hemisphere is slightly compressed on a flat plane. However, this technique is not suitable for highly compliant materials or structures for which deformations become non-linear. Here we experimentally explore an alternative approach, inspired from the compliance method originally developed for fracture mechanics and based on the measurement of the work of adhesion during an indentation cycle. We illustrate this technique with elastomeric hemispherical shells and propose an extension to non axisymmetric shapes. Although the involved forces are of the same order of magnitude as in a standard JKR test, the corresponding displacements are much larger and can thus be more easily controlled. Precise measurements of adhesion then become possible on samples of arbitrary shape or internal structure and materials with non-linear elastic response.

1 Introduction

Étienne Guyon deeply enjoyed human interactions and scientific discussions. After a dense carrier in prestigious institutions, Étienne chose to return to the PMMH lab he founded in the late 1970s. He then shared a cosy office with our colleague Michel Barquins (1941–2024), a brilliant specialist in adhesion and friction with a lively personality. Discussions with Étienne and Michel certainly partly inspired the following work. Étienne was also very involved in making connections and diffusing physics across oceans. He was particularly involved in the development of scientific programs on non-linear physics in Chile, promoting regular exchanges between Paris and Santiago. Two of the authors of this work illustrate the deep value of such exchanges. Finally, Étienne also made a point that things and scientific concepts should be named properly. When co-writing a book on the physics and mechanics of Hidden Wonders around us, he insisted that adherence and adhesion are two different concepts [1]. The latter is discussed in the present paper: we explore a simple method based on basic force and contact area monitoring to assess adhesion energy of highly compliant structures.

Indentation tests are commonly used to measure adhesion between materials. The standard "JKR" test consists in extracting the adhesion energy from a measurement of the force resulting from the indentation of an elastic sphere on a rigid plate [2]. This method is based on a theoretical description of the process through linear elasticity, which assumes small deformations. However, many adhering strategies found in Nature rely on highly compliant substrates, which enhances contact between adhering surfaces and thus promotes good adhesion. For instance, flexible *setae* present at the extremities of geckos toes are responsible for their remarkable adhesive properties [3].

[a] e-mail: miguel.trejo.l@gmail.com
[b] e-mail: suomiponce@protonmail.com
[c] e-mail: jose.bico@espci.fr
[d] e-mail: etienne.reyssat@espci.fr (corresponding author)
[e] e-mail: benoit.roman@espci.fr
[f] e-mail: ch45@cornell.edu

Published online: 19 September 2025

Similar flexible adhesive structures are also present on the legs of various species of insects or spiders [4]. These adhering strategies have motivated the development of novel bio-inspired microstructured materials with the aim of improving the adhesive strength of engineered systems such as dry adhesives tapes [5–8] or clamps for soft robots [9, 10]. Beyond animal locomotion, adhesion of soft tissues or membranes also plays a crucial role in life science, such as the adhesion of vesicles [11, 12] or of cells [13–16].

Although the JKR framework has been reviewed and extended to account for large deformations and non-linear elasticity [17–19], probing very soft materials, such as biological tissues remains delicate. Similarly, adapting this standard test to slender structures such as adhesive loops [20] or shells is a difficult task due to both the large deformations, buckling and, more generally, geometrical non-linearities involved in indentation [21–25]. Most methods derived from the JKR framework rely on the analytical or numerical modelling of the elastic energy stored in the samples during indentation or release, which requires to know the mechanical properties of the material and to carefully take into account the details of the geometry of the experiment [26–28]. In contrast, the technique discussed in the present work does not require analytical or numerical developments involving the constitutive law of the material or structure probed. However, it requires to measure the contact area precisely.

We experimentally revisit an alternative approach to infer the adhesion energy, inspired from the *compliance method* [18] which relies on a graphical method proposed by Berry [29] and later popularised by Maugis [30]. It has been previously studied, both experimentally and theoretically to assess fracture energy of full solid spheres [31] and fibrillar surfaces [32], and only theoretically for slender structures [33]. Here we explore and verify the validity of these concepts with the indentation of thin hyperelastic hemispherical shells.

The method is based on the integration of the force-displacement curves during hysteretic indentation cycles. Provided there is no energy loss through plasticity or snapping instabilities, the adhesion energy is inferred from the increment of the corresponding mechanical work between successive cycles.

2 Experimental

Soft elastic shells are fabricated by following the technique proposed by Lee et al. [34]. Preparations of 1:1 liquid "base" and "catalyst" of vinyl-polysiloxane (Elite Double 8 from Zhermack, referred to as VPS08) are poured on smooth solid spheres of radius R ranging from 5 to 25 mm. After a curing time of typically 20 min at room temperature, the sphere is removed, leaving a hemispherical shell of almost uniform thickness h ranging from 80 to 250 µm (see Fig. 1). Prior to experiment, potential dust particles are removed from the shells with a standard adhesive tape. The shells were then cleaned with isopropanol, as well as the glass plate used as indenting substrate.

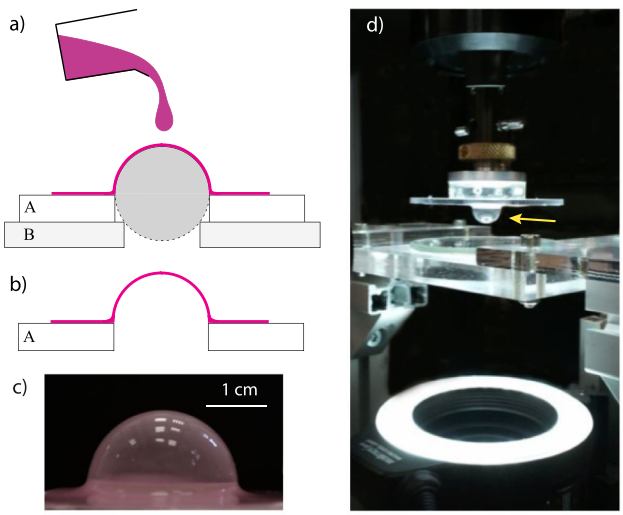

Fig. 1 Description of procedure used to produce the hemispherical shells. **a** Two concentric annular plates (A and B) support a solid sphere over which liquid uncured polymer is poured. **b** Final solid shell, plate B has been removed as well the solid sphere when the cross-linking reaction is finished. **c** Picture of a typical shell used in our experiments. Its thickness is on the order of 100 µm. **d** Experimental setup. In the center of the image, an inverted hemispherical shell pointed by the yellow arrow is supported on an acrylic plate. This plate is mounted on the load cell of a force-displacement machine. Side and bottom view images are recorded during the complete indentation process with a typical interval of 3 s

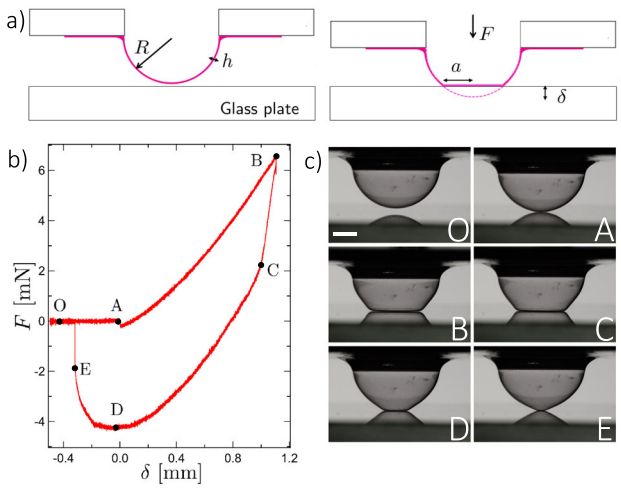

Fig. 2 **a** Sketch of the shell indentation experiment. A hemispherical shell (radius R, thickness h) is approached at a constant velocity V towards a glass plate. When both surfaces get into contact, the resulting force F and the contact radius a are monitored as a function of the imposed indentation δ. **b** Force vs displacement curve for an adhesive shell with Young modulus $E = 220 \pm 1.1$ kPa, $R = 7.0 \pm 0.1$ mm, $h = 98 \pm 4\,\mu$m and $V = 0.1$ mm/min. **c** Side views of the shell at different stages O, A, B, C, D, E (white scalebar 2 mm)

The support holding the soft shell is mounted on the load cell of a force-displacement machine (Instron 5865) as illustrated in Fig. 1d. Indentation is performed at controlled displacement, sometimes referred to as fixed-grips, with a sensitivity 10–100 nm and at a constant velocity V between 0.01 and 1 mm/min. During the indentation process, the instantaneous force F on the shell is monitored as a function of the imposed displacement δ. The radius of the contact region is simultaneously recorded by imaging the contact with a camera placed under the glass plate. Although the work of adhesion of elastomers is known to vary with the peeling front velocity at the contact line [35], preliminary tests indicate that the force-displacement curves did not vary significantly within the experimental range of indentation velocity. All following indentation tests were thus conducted at a velocity $V = 0.1$ mm/min. In parallel to shells, solid spheres of the same elastomer are prepared to conduct standard JKR tests as described in Appendix A. For the same indentation velocity, we measure a work of adhesion of $\gamma = 0.100 \pm 0.050$ J/m^2 for VPS08 on glass, which is a typical value for the relatively weak van der Waals intermolecular adhesion of silicone-based elastomers on glass [36–38]. Additionally, the Young modulus of the cured elastomer was also measured as $E = 220 \pm 1.1$ kPa, which is coherent with a previously reported value obtained using a tensile test on a strip [39].

We present in Fig. 2b a force vs displacement plot for a typical shell. Once the contact is established (point A), the force increases monotonically between points A and B. The contact area is circular and the shell is slightly deformed (but does not buckle) on the non-contacting zone. The maximal indentation $\delta_m \sim 1$ mm is reached at point B. After a dwell time of 3 min, the shell is pulled out. Initially the force decreases, mostly relaxing the elastic energy stored in the deformed shell, but with a constant contact area. Beyond point C, a local peeling process along the perimeter of the circular contact area is observed. The force continues to decrease, passes through zero and becomes negative as the shell gets under tension. The force eventually reaches a minimum value (point D). The shell finally detaches from the plate (point E) and the force suddenly jumps to zero.

The global shape of the curve is reminiscent of the standard JKR case of the solid sphere with a strong hysteresis between the loading and unloading regimes. However, although the amplitude of the force remains of the same order in both configurations, the corresponding indentation displacement is 2 orders of magnitude larger in the case of the shell.

3 Discussion

Can adhesive properties be inferred from a simple indentation test on a shell? In contrast with the case of the solid hemisphere, the deformation of the shell is highly non-linear and the work of adhesion cannot be readily estimated through an analytic expression as in the JKR framework. We experimentally explore an alternative technique based on the comparison of different loading cycles, as inspired by the theoretical framework developed by Hui and Long [33]. Consider a set of indentation cycles with increment of the maximum displacement $\Delta\delta_m = 100$ µm, as shown in Fig. 3a. Each cycle starts with a quasi-static loading phase where contact progresses everywhere (from the starting point S to B). The contact area increases monotonically and reaches a maximum $\mathcal{A}_m$, involving

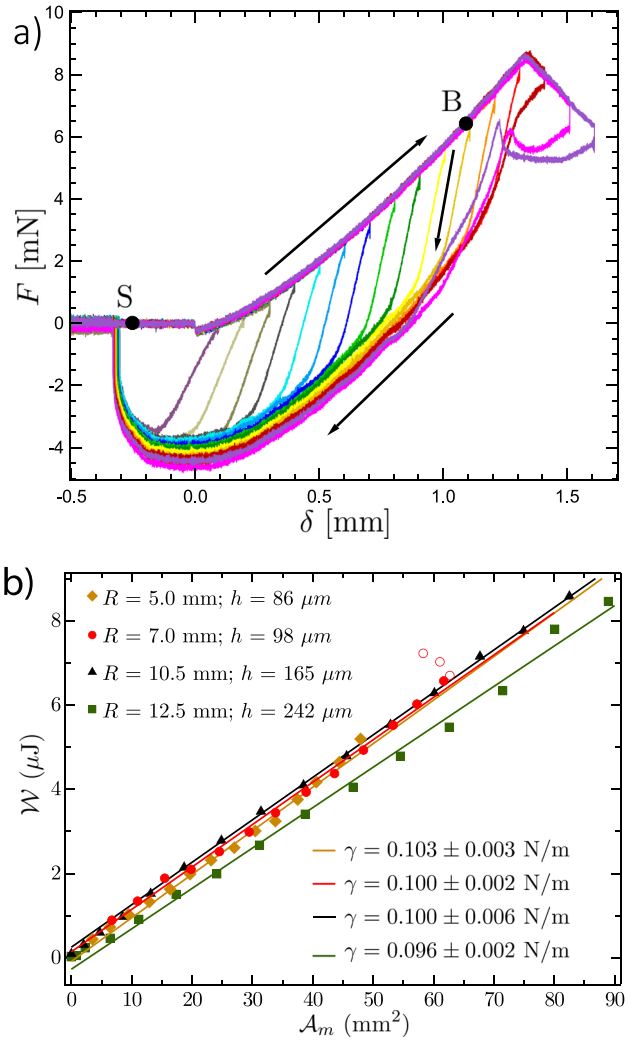

Fig. 3 **a** Comparison of indentation cycles for VPS08 material on glass ($E = 220$ kPa, $R = 7.0$ mm, $h = 98 \pm 4\,\mu$m, $V = 0.1$ mm/min, $\Delta\delta_m = 100\,\mu$m). S is the starting point of all cycles and B indicates the point of maximum contact area, at which displacement is reversed during the cycle. The irregular behavior of the last cycles corresponds to a buckling transition of the shell. Similar data for shells of different radii and thicknesses are shown in Appendix B. **b** Work inferred from the integration of the force-displacement curve over cycles of increasing amplitude as a function of the maximum contact area, for shells of various radii and thicknesses. The indentation velocity is $V = 0.1$ mm/min for all experiments. The slope of the best fit to the data gives us the work of adhesion for the systems VPS08/glass ($\gamma \simeq 0.1$ N/m), and it is shown to be independent of geometry. The data points corresponding to buckling (hollow symbols) are clearly off this linear trend and have been disregarded

a gain of adhesion energy $\gamma_{\rm adv}\mathcal{A}_m$. During the release phase, contact recedes (from B back to S) and the system absorbs the adhesion energy $\gamma_{\rm rec}\mathcal{A}_m$. We assume that during the quasi-static phases of a cycle, the energy loss in the system arises solely from the difference in adhesion energies $\gamma_{\rm adv}$ and $\gamma_{\rm rec}$. In particular, large values of the peeling angle during the unloading process ensure that the shell barely slides along the substrate, so that losses by friction can be neglected [40–43]. During loading, part of the work done by the apparatus is stored into elastic deformations of the shell. Most of it is returned during unloading, except for a small part that could be dissipated during the final snap-off event. This excess dissipation could occur during the final debonding process, this phase is common to all cycles. Thus, the work $\mathcal{W} = \int F(\delta)\mathrm{d}\delta$ provided to the system during a cycle reads

$$\mathcal{W} = (\gamma_{\rm rec} - \gamma_{\rm adv})\mathcal{A}_m + \mathcal{W}_0 \tag{1}$$

where $\mathcal{W}_0$ is a small offset common to all cycles and associated to the release of elastic energy during the final detachment which depends on the geometrical and mechanical properties of the sample. The interfacial processes involved in the loading and release phases usually correspond to adhesion energies $\gamma_{\rm adv}$ and $\gamma_{\rm rec}$ of very different

amplitudes. We thus assume $\gamma_{\mathrm{adv}} \ll \gamma_{\mathrm{rec}}$ as it is the case in most practical cases [18]. This hypothesis is further confirmed with a test conducted on shells covered with talc powder, which suppresses adhesion and hysteresis in the cycles. Finally, the work provided to the system over one cycle is

$$\mathcal{W} = \gamma \mathcal{A}_m + \mathcal{W}_0 \tag{2}$$

where $\gamma \simeq \gamma_{\mathrm{rec}}$ is the adhesion energy per unit surface, also referred to as "work of adhesion".

To validate this theoretical approach, we show in Fig. 3b that $\mathcal{W}$ grows linearly with the maximal contact area $\mathcal{A}_m$ for the different loading cycles. The data follows a straight line of slope $\gamma = 0.100 \pm 0.002$ N/m except for the largest indentation data points, where the shell has undergone a buckling instability (open circles in Fig. 3b). The buckling instability observed for high loads is presented in more details in Appendix B (see Fig. 7). This measurement of the work of adhesion is thus in good agreement with independent estimates from a classical JKR test on a solid sphere, which give $\gamma = 0.100 \pm 0.050$ N/m (see Appendix A). It is also much more precise, thanks to the large displacements involved upon indentation of such very soft thin shells.

The measurements for shells of various radii and thicknesses lead to curves of similar slopes (Fig. 3b), which further confirms the modeling hypothesis. Note that in these measurements, we have taken special care in measuring adhesion on fresh samples a few minutes after curing the elastomer. Aging over hours tends to decrease the value of γ to typically 0.080 N/m both in JKR and thin shell measurements.

We also probed substrates of different adhesion energies. We first grafted trichloroperfluorooctylsilane molecules following the standard technique described in detail by Mettu and Chaudhury [44]. A second set of experiments was conducted with a glass plate coated with a very thin layer of the same VPS08 polymer. This film is obtained by spin coating a small quantity of the uncrosslinked polymer at 3000 rpm for 30 s. The thickness of the coating is on the order of 10 µm, i.e. typically ten times thinner than the shell, so that the substrate remains essentially undeformed during the experiments. The results obtained with the different substrates are compared in Fig. 4. We observe an increase of the work of adhesion for the silanized surface ($\gamma = 0.160 \pm 0.003$ N/m). Conversely, the VPS08/VPS08 contact displays a lower work of adhesion $\gamma = 0.040 \pm 0.007$ N/m, which is in qualitative agreement with classical experiments conducted with polydimethylsiloxane substrates [36].

In order to explore the generality of this approach, we have conducted experiments with non-axisymmetric shells. To produce such shells we poured the liquid polymer on ellipsoidal objects instead of regular spheres. The thickness of the resulting shells is not uniform, which should nevertheless not affect the estimate of the work of adhesion as the theoretical procedure does not depend on the actual geometrical properties of the shells. We tested two different shapes. A first specimen was obtained by pouring the liquid polymer on an ovoid template leading to a prolate ellipsoid of semi-axes of 9.5 and 7.5 mm and a height of 7.5 mm. The radius of curvature at the axisymmetric apex is 5 mm. A second specimen was obtained by molding a capsule (a cylinder with rounded ends), leading to an oblate shell of semi-axes of 5 and 10 mm and a height of 5 mm (insets in Fig. 5). Both shells have a thickness on the order of 100 µm. In Fig. 5, we plot the evolution of work furnished during a series of indentation cycles as a function of the maximal contact area. Both curves follow the same line. We estimate the work of adhesion from a linear fit $\gamma = 0.08 \pm 0.02$ [N/m]. Both measurements are consistent, independently of the shell geometry, and we interpret the minor mismatch with measurements in Fig. 3 (γ is on the order of 10–20% lower here) as a consequence of aging of the polymer for about 2 weeks before performing the adhesion test.

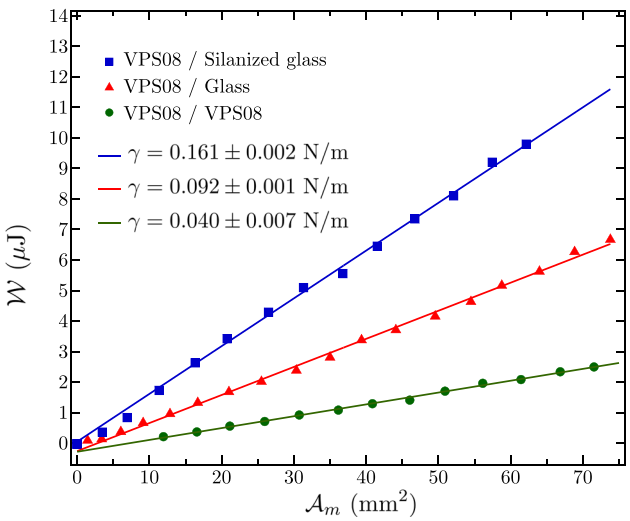

Fig. 4 Comparison of the integrated force for glass plates with different surface properties. The geometry of the VPS08 shell is fixed ($R = 7.5$ mm, $h = 113 \pm 4$ µm). While the variation of $\mathcal{W}$ with $\mathcal{A}_m$ remains linear, we measure an increased work of adhesion with a glass plate grafted with a fluorinated silane ($\gamma = 0.160 \pm 0.003$ N/m) and a lower value for a plate coated with a thin layer of the same VPS08 material

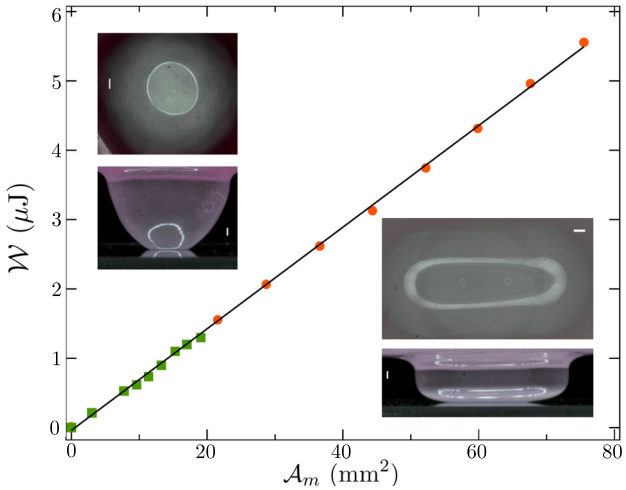

Fig. 5 Work under the curves $\mathcal{W}$ calculated using the indentation experiments in non-axisymmetric shells of VPS08 ($E = 220$ kPa, $h = 100\,\mu$m, at $V = 0.1$ mm/min). Prolate (Ovoid) (green squares) and oblate (capsule) shapes (red circles) and, $\gamma = 0.08 \pm 0.02$ N/m given by the black curve slope. Upper insets: view of the contact areas. Bottom insets: side view of the shells

4 Conclusion

As a conclusion, we have proposed a versatile procedure to measure the interfacial work of adhesion for slender structures or soft materials. This method simply consists in integrating the loading force during a standard indentation cycle and plotting this work $\mathcal{W}$ as a function of the maximum contact area $\mathcal{A}_m$. Interestingly, the derivation of the work of adhesion does not depend on the non-linear elastic response of the structure, nor on the constitutive stress–strain law of the material. Although we have illustrated the validity of the technique for hemispherical and ellipsoidal shells, this is, in principle, valid with any other type of geometry for a slender structure. As the displacements involved in loading the specimens are typically two orders of magnitude higher than in conventional JKR tests, the method does not require a very accurate vertical positioning of the probe, but needs a precise monitoring of the contact area at maximal indentation.

The procedure relies on several assumptions: (i) the adhesion energy for an advancing front is negligible in comparison with a receding front: $\gamma_{\text{adv}} \ll \gamma_{\text{rec}}$; (ii) while the material response can be non-linear, it must remain elastic and should not involve any plasticity, visco-elastic dissipation or friction; (iii) during indentation cycles, the boundary of the contact zone must first advance everywhere during indentation and then recede everywhere during unloading. This last assumption may fail for the deepest indentations in our experiments: as the shell buckles, the adhesion front may locally recede even though δ keeps increasing (see Fig. 7 in Appendix B). Visco-elastic dissipation, or even self adhesion may also occur during this fast change of shape of the shell.

Finally, as this method is independent of the geometrical and mechanical properties of the two materials in contact (homogeneity, anisotropy), it could be relevant to measure the adhesion energy between complex soft objects which cannot be assessed through standard JKR tests.

Acknowledgements We thank Thomas Salez and Élie Raphaël for stimulating discussions. This research was partially funded by the Interuniversity Attraction Poles Programme (MicroMAST) initiated by the Belgian Science Policy Office and the French ANR SMART. Chaire Total-ESPCI has funded the stay of C.-Y. Hui.

Data availability The data that support the findings of this study are available from the corresponding author, E.R., upon reasonable request.

Declarations

Conflict of interest The authors declare no Conflict of interest.

Appendix A Reference JKR tests on solid hemispheres

Before probing shells, standard JKR tests were conducted on solid hemispheres in order to extract the adhesion energy of VPS elastomers on glass. These hemispheres were readily obtained by molding rigid acrylic shells (commercial decorating balls). The protocol is composed of three steps:

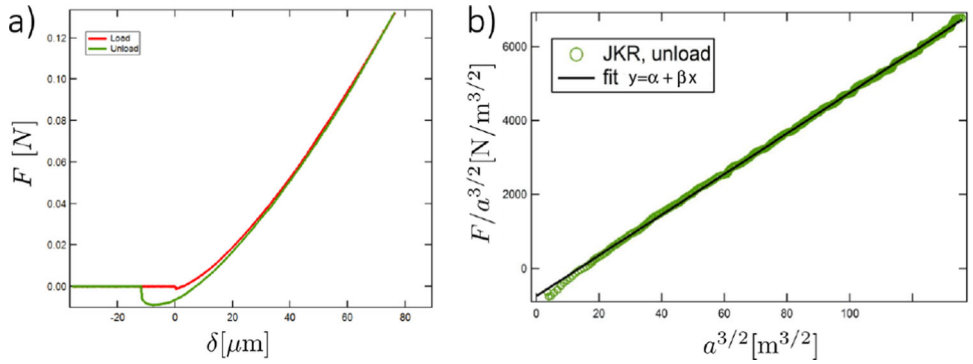

Fig. 6 Typical JKR indentation test with a plain shell of VPS 08 ($R = 7.5$ mm at $V = 0.1$ mm/min). **a** Force displacement curves. Red plot: loading regime where adhesion is negligible as in Hertz classical law. Green plot: unloading regime where adhesion results in a finite contact area at zero force. **b** $F/a^{3/2}$ versus a function of $a^{3/2}$ in the unloading regime. Following JKR theory this plot corresponds to a straight line (black line) of slope $4E^*/3R$ and intercept $-2\sqrt{2\pi\, E^*\gamma}$. We can infer from this data set the work of adhesion, $\gamma = 0.1 \pm 0.05\,\mathrm{J/m^2}$

(i) loading at a constant velocity V up to a maximum indentation δ_m,
(ii) dwelling time $t_w = 3$ min during which the sample is maintained in contact with the substrate,
(iii) unloading at the same velocity V.

A typical force vs displacement plot is displayed in Figure 6a. Two behaviors are successively observed during the test. In the loading regime, the force follows the classical Hertz law where adhesion is neglected:

$$F_H(\delta) = \frac{4\,E^*}{3\,R}\left(\frac{\delta}{R}\right)^{3/2} \tag{A1}$$

where R is the radius of the sphere and $E^* = E/(1-\nu^2)$ is the reduced elastic modulus, with E the Young modulus and ν the Poisson ratio.

A strong hysteresis is observed during unloading, as adhesion energy tends to retain the contact of the hemisphere on the substrate. In this regime, the applied force is expected to follow the JKR model, which accounts for adhesion [2]:

$$F(a) = F_H(a) - 2\sqrt{2\pi E^*\gamma}\; a^{3/2}, \qquad F_H(a) = \frac{4E^*}{3R}a^3, \tag{A2}$$

$$\delta(a) = \delta_H(a) - \sqrt{\frac{2\pi\gamma}{E^*}}\; a^{1/2}, \qquad \delta_H(a) = \frac{a^2}{R}, \tag{A3}$$

where a is the contact radius and γ the work of adhesion. The "H" subscript refers to Hertz law which is recovered by turning off the adhesion. Following JKR expression, a plot of $F/a^{3/2}$ versus $a^{3/2}$ corresponds to a line of slope $4E^*/3R$ and intercept $-2\sqrt{2\pi\, E^*\gamma}$. In Fig. 6b we show the result of the unloading process analyzed by using this equation. We obtain $E = 220 \pm 1.1$ kPa and $\gamma = 0.1 \pm 0.05\,\mathrm{J/m^2}$, for VPS-08 elastomer. In terms of order of magnitude, typical values of the displacement and contact radius at no charge and of the maximum pulling force (in absolute value) are respectively given by $\delta_0 \sim \left(\frac{\gamma^2 R}{E^{*2}}\right)^{1/3} \sim 10\,\mu\mathrm{m}$, $a_0 \sim \left(\frac{\gamma R^2}{E^*}\right)^{1/3} \sim 200\,\mu\mathrm{m}$ and $F_{\min} \sim \gamma R \sim 4$ mN.

Appendix B Buckling

The shells used in our experiments tend to buckle for large values of the indentation. Before buckling, we observe that the maximum contact area A_m varies linearly with the maximum indentation δ_m (Fig. 7a). This behavior

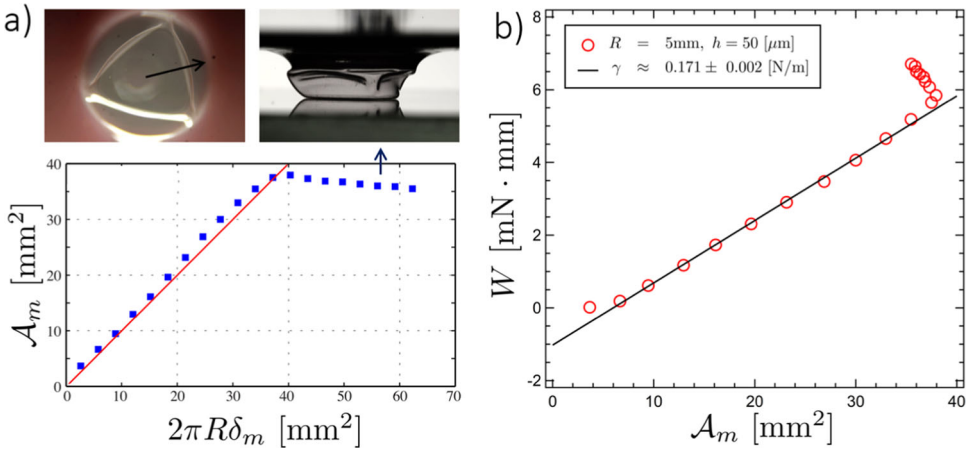

Fig. 7 Post-buckling cycles. **a** Maximal contact area $\mathcal{A}_m$ as a function of the maximal indentation depth δ_m for a given set of cycles. The red line corresponds to the geometrical relation $\mathcal{A}_m = 2\pi R\delta_m$. Note that the maximal contact area slightly decreases at the onset of buckling. **b** Integrated work for successive cycles as a function of the maximal area (VPS 08 material: $E = 220$ kPa, $R = 5.0$ mm, $h \simeq 50\,\mu$m, $\Delta\delta = 100\,\mu$m, indentation rate $V = 0.1$ mm/min. Data away from the straight line correspond to post-buckling cycles

can be described with a simple geometrical relation where adhesion is neglected:

$$\delta_m = R\left(1 - \sqrt{1 - \left(\frac{a_m}{R}\right)^2}\right) \simeq \frac{a_m^2}{2R} \quad \text{for} \quad a_m \ll R$$

where a_m is the radius of the contact zone (in the absence of buckling). Considering area of contact $A_m = \pi a_m^2$, we obtain:

$$A_m \simeq 2\pi R\delta_m \tag{B4}$$

This expression corresponds to the red dotted line in (Fig. 7a) and is in good agreement with experimental data before buckling occurs. As a consequence of buckling, the evolution of the work integrated on a cycle does not follow our theoretical prediction. Buckling induces additional dissipation such as visco-elastic effects during the fast change of shape of the shell, self adhesion involving friction, heterogeneous adhesion front where some parts may advance while the other recede (the contact zone may lose its circularity).

Buckling deformations thus constitute a limitation to our procedure. Nevertheless, the corresponding data points can readily be identified, since the contact area tends to slightly decrease and saturate after buckling.

References

1. E. Guyon, J. Bico, E. Reyssat, B. Roman, *Hidden Wonders: The Subtle Dialogue Between Physics and Elegance* (MIT Press, Boston, 2021)
2. K.L. Johnson, K. Kendall, A.D. Roberts, D. Tabor, Surface energy and the contact of elastic solids. Proc. R. Soc. Lond. A Math. Phys. Sci. **324**(1558), 301–313 (1971). https://doi.org/10.1098/rspa.1971.0141
3. K. Autumn, Y.A. Liang, S.T. Hsieh, W. Zesch, W.P. Chan, T.W. Kenny, R. Fearing, R.J. Full, Adhesive force of a single gecko foot-hair. Nature **405**(6787), 681–685 (2000). https://doi.org/10.1038/35015073
4. E. Arzt, S. Gorb, R. Spolenak, From micro to nano contacts in biological attachment devices. Proc. Natl. Acad. Sci. **100**(19), 10603–10606 (2003). https://doi.org/10.1073/pnas.1534701100
5. N.J. Glassmaker, A. Jagota, C.-Y. Hui, W.L. Noderer, M.K. Chaudhury, Biologically inspired crack trapping for enhanced adhesion. Proc. Natl. Acad. Sci. **104**(26), 10786–10791 (2007). https://doi.org/10.1073/pnas.0703762104
6. A. Jagota, C.-Y. Hui, Adhesion, friction, and compliance of bio-mimetic and bio-inspired structured interfaces. Mater. Sci. Eng., R **72**(12), 253–292 (2011). https://doi.org/10.1016/j.mser.2011.08.001
7. C. Poulard, F. Restagno, R. Weil, L. Leger, Mechanical tuning of adhesion through micro-patterning of elastic surfaces. Soft Matter **7**, 2543–2551 (2011). https://doi.org/10.1039/C0SM01099E
8. M.D. Bartlett, A.B. Croll, A.J. Crosby, Designing bio-inspired adhesives for shear loading: from simple structures to complex patterns. Adv. Funct. Mater. **22**(23), 4985–4992 (2012). https://doi.org/10.1002/adfm.201201344

9. L. Heepe, S.N. Gorb, Biologically inspired mushroom-shaped adhesive microstructures. Annu. Rev. Mater. Res. **44**, 173–203 (2014). https://doi.org/10.1146/annurev-matsci-062910-100458
10. D. Brodoceanu, C.T. Bauer, E. Kroner, E. Arzt, T. Kraus, Hierarchical bioinspired adhesive surfaces, a review. Bioinspir. Biomim. **11**(5), 051001 (2016). https://doi.org/10.1088/1748-3190/11/5/051001
11. E. Evans, D. Needham, Attraction between lipid bilayer membranes in concentrated solutions of nonadsorbing polymers: comparison of mean-field theory with measurements of adhesion energy. Macromolecules **21**(6), 1822–1831 (1988). https://doi.org/10.1021/ma00184a049
12. Y. Lin, L.B. Freund, Forced detachment of a vesicle in adhesive contact with a substrate. Int. J. Solids Struct. **44**(6), 1927–1938 (2007). https://doi.org/10.1016/j.ijsolstr.2006.09.006
13. N. Wang, D.E. Ingber, Control of cytoskeletal mechanics by extracellular matrix, cell shape, and mechanical tension. Biophys. J. **66**(6), 2181 (1994). https://doi.org/10.1016/S0006-3495(94)81014-8
14. J.-Y. Shao, G. Xu, P. Guo, Quantifying cell-adhesion strength with micropipette manipulation: principle and application. Front. Biosci. **9**, 2183–2191 (2004). https://doi.org/10.2741/1386
15. Y.-S. Chu, S. Dufour, J.P. Thiery, E. Perez, F. Pincet, Johnson–Kendall–Roberts theory applied to living cells. Phys. Rev. Lett. **94**(2), 028102 (2005). https://doi.org/10.1103/PhysRevLett.94.028102
16. M.-J. Colbert, F. Brochard-Wyart, C. Fradin, K. Dalnoki-Veress, Squeezing and detachment of living cells. Biophys. J . **99**(11), 3555–3562 (2010). https://doi.org/10.1016/j.bpj.2010.10.008
17. K.R. Shull, D. Ahn, W.-L. Chen, C.M. Flanigan, A.J. Crosby, Axisymmetric adhesion tests of soft materials. Macromol. Chem. Phys. **199**(4), 489–511 (1998). https://doi.org/10.1002/(SICI)1521-3935(19980401)199:4<489::AID-MACP489>3.0.CO;2-A
18. K.R. Shull, Contact mechanics and the adhesion of soft solids. Mater. Sci. Eng. R. Rep. **36**(1), 1–45 (2002). https://doi.org/10.1016/S0927-796X(01)00039-0
19. Y.-Y. Lin, H.-Y. Chen, Effect of large deformation and material nonlinearity on the JKR (Johnson–Kendall–Roberts) test of soft elastic materials. J. Polym. Sci. B **44**(19), 2912–2922 (2006). https://doi.org/10.1002/polb.20914
20. T. Elder, T. Twohig, H. Singh, A.B. Croll, Adhesion of a tape loop. Soft Matter **16**(47), 10611–10619 (2020). https://doi.org/10.1039/D0SM01516D
21. L. Pauchard, S. Rica, Contact and compression of elastic spherical shells: the physics of a 'ping-pong' ball. Philos. Mag. B **78**(2), 225–233 (1998). https://doi.org/10.1080/13642819808202945
22. S. Komura, K. Tamura, T. Kato, Buckling of spherical shells adhering onto a rigid substrate. Eur. Phys. J. E **18**(3), 343 (2005). https://doi.org/10.1140/epje/e2005-00038-5
23. A. Vaziri, L. Mahadevan, Localized and extended deformations of elastic shells. Proc. Natl. Acad. Sci. **105**(23), 7913–7918 (2008). https://doi.org/10.1073/pnas.0707364105
24. C. Quilliet, C. Zoldesi, C. Riera, A. Blaaderen, A. Imhof, Anisotropic colloids through non-trivial buckling. Eur. Phys. J. E **27**(1), 13–20 (2008). https://doi.org/10.1140/epje/i2007-10365-2
25. N.P. Bende, A.A. Evans, S. Innes-Gold, L.A. Marin, I. Cohen, R.C. Hayward, C.D. Santangelo, Geometrically controlled snapping transitions in shells with curved creases. Proc. Natl. Acad. Sci. **112**(36), 11175–11180 (2015). https://doi.org/10.1073/pnas.1509228112
26. S.M. Jiayi Shi, K.-T. Wan, Adhesion of an elastic convex shell onto a rigid plate. J. Adhes. **87**(6), 579–594 (2011). https://doi.org/10.1080/00218464.2011.583587
27. A.G. Jiayi Shi, S. Müftü, K.-T. Wan, Adhesion of a cylindrical shell in the presence of DLVO surface potential. J. Appl. Mech. **80**, 061007 (2013). https://doi.org/10.1115/1.4023960
28. C. Zhao, X. Chen, W. Shan, K.-T. Wan, Adherence of a hyperelastic shell on a rigid planar substrate. Int. J. Solids Struct. **236–237**, 111351 (2022). https://doi.org/10.1016/j.ijsolstr.2021.111351
29. J.P. Berry, Some kinetic considerations of the Griffith criterion for fracture—I. Equations of motion at constant force. J. Mech. Phys. Solids **8**, 194–206 (1960). https://doi.org/10.1016/0022-5096(60)90038-7
30. D. Maugis, *Contact, Adhesion and Rupture of Elastic Solids* (Springer, Heidelberg, 2000)
31. S. Vajpayee, C.-Y. Hui, A. Jagota, Model-independent extraction of adhesion energy from indentation experiments. Langmuir **24**(17), 9401–9409 (2008). https://doi.org/10.1021/la800817x
32. W. Noderer, L. Shen, S. Vajpayee, N. Glassmaker, A. Jagota, C.-Y. Hui, Enhanced adhesion and compliance of film-terminated fibrillar surfaces. Proc. R. Soc. A. Math. Phys. Eng. Sci. **463**(2086), 2631–2654 (2007). https://doi.org/10.1098/rspa.2007.1891
33. C.-Y. Hui, R. Long, Direct extraction of work of adhesion from contact experiments: generalization of JKR theory to flexible structures and large deformation. J. Adhes. **88**(1), 70–85 (2012). https://doi.org/10.1080/00218464.2011.611090
34. A. Lee, P.-T. Brun, J. Marthelot, G. Balestra, F. Gallaire, P.M. Reis, Fabrication of slender elastic shells by the coating of curved surfaces. Nat. Commun. **7**, 1–7 (2016). https://doi.org/10.1038/ncomms11155
35. K. Kendall, Thin-film peeling-the elastic term. J. Phys. D **8**(13), 1449 (1975). https://doi.org/10.1088/0022-3727/8/13/005
36. M.K. Chaudhury, G.M. Whitesides, Direct measurement of interfacial interactions between semispherical lenses and flat sheets of poly (dimethylsiloxane) and their chemical derivatives. Langmuir **7**(5), 1013–1025 (1991). https://doi.org/10.1021/la00053a033
37. Y. Yu, D. Sanchez, N. Lu, Work of adhesion/separation between soft elastomers of different mixing ratios. J. Mater. Res. **30**(18), 2702–2712 (2015). https://doi.org/10.1557/jmr.2015.242
38. L.F.M. Silva, A. Öschner, R.D. Adams, *Handbook of Adhesion* (Springer, Berlin, 2011)

39. H. Bense, M. Trejo, E. Reyssat, J. Bico, B. Roman, Buckling of elastomer sheets under non-uniform electro-actuation. Soft Matter **13**(15), 2876–2885 (2017). https://doi.org/10.1039/C7SM00131B
40. M. Barquins, Adherence, friction and contact geometry of a rigid cylinder rolling on the flat and smooth surface of an elastic body (NR and SBR). J. Nat. Rubber Res. (1990)
41. B.-M.Z. Newby, M.K. Chaudhury, Friction in adhesion. Langmuir **14**(17), 4865–4872 (1998). https://doi.org/10.1021/la980290l
42. M. Trejo, C. Fretigny, A. Chateauminois, Friction of viscoelastic elastomers with rough surfaces under torsional contact conditions. Phys. Rev. E **88**(5), 052401 (2013). https://doi.org/10.1103/PhysRevE.88.052401
43. S. Ponce, J. Bico, B. Roman, Effect of friction on the peeling test at zero-degrees. Soft Matter **11**(48), 9281–9290 (2015). https://doi.org/10.1039/C5SM01203A
44. S. Mettu, M.K. Chaudhury, Motion of liquid drops on surfaces induced by asymmetric vibration: role of contact angle hysteresis. Langmuir **27**(16), 10327–10333 (2011). https://doi.org/10.1021/la201597c

Springer Nature or its licensor (e.g. a society or other partner) holds exclusive rights to this article under a publishing agreement with the author(s) or other rightsholder(s); author self-archiving of the accepted manuscript version of this article is solely governed by the terms of such publishing agreement and applicable law.